Effects of Vessel Geometry and Catheter Position on Dose Delivery in Intracoronary Brachytherapy

Andreas Wahle,* *Senior Member, IEEE*, John J. Lopez, Edward C. Pennington, Sanford L. Meeks, Kathleen C. Braddy, James M. Fox, Theresa M. H. Brennan, John M. Buatti, James D. Rossen, and Milan Sonka, *Fellow, IEEE*

***Abstract*—In-stent restenosis is commonly observed in coronary arteries after intervention. Intravascular brachytherapy has been found effective in reducing the recurrence of restenosis after stent placement. Conventional dosing models for brachytherapy with beta (β) radiation neglect vessel geometry as well as the position of the delivery catheter. This paper demonstrates in computer simulations on phantoms and on in-vivo patient data that the estimated dose distribution varies substantially in curved vessels. In simulated phantoms of 50 mm length with a shape corresponding to a 60–180° segment of a respectively sized torus, the average dose in 2 mm depth was decreased by 2.70–7.48% at the outer curvature and increased by 2.95–9.70% at the inner curvature as compared to a straight phantom. In-vivo data were represented in a geometrically correct three-dimensional model that was derived by fusion of intravascular ultrasound (IVUS) and biplane angiography. These data were compared to a simplified tubular model reflecting common assumptions of conventional dosing schemes. The simplified model yielded significantly lower estimates of the delivered radiation and the dose variability as compared to a geometrically correct model ($p < 0.001$). The estimated dose in 10 vessel segments of 8 patients was on average 8.76% lower at the lumen/plaque and 6.52% lower at the media/adventitia interfaces (simplified tubular model relative to geometrically correct model). The differences in dose estimates between the two models were significantly higher in the right coronary artery as compared to the left coronary artery ($p < 0.001$).**

***Index Terms*— Coronary atherosclerosis, in-stent restenosis, intravascular brachytherapy, dose-distribution models, multimodality imaging.**

I. Introduction

CORONARY atherosclerosis is a widespread disease, resulting in plaque accumulation and narrowing of the vessel lumen (stenosis). Treatment of local coronary artery stenoses usually involves dilatation of the vessel lumen by percutaneous transluminal coronary angioplasty (PTCA) and stent placement [1]. In this procedure, a stainless steel stent mounted on an angioplasty balloon is inserted into the vessel lumen and inflated, thus widening the obstructed area by compressing plaque and expanding the media-adventitial border. Despite a successful initial procedure, 20–30% of patients return with clinical symptoms and sequelae due to neointimal formation with a previously placed stent, resulting in *in-stent restenosis* [2]. This process can be observed using intravascular ultrasound (IVUS) as demonstrated in Figure 1. To reduce the incidence of repeat restenosis, intravascular brachytherapy with either beta (β) or gamma (γ) radiation has been shown to be effective after repeat balloon dilation [3]–[5]. A comprehensive tutorial-style review can be found in [6]. In-stent restenosis was also analyzed in porcine and more recently rat studies [7]–[9]. The typical approach involves a catheter that is delivered to the treatment site within the stented region. A train of β-seeds or a γ-wire is sent to the treatment site, where it dwells for a calculated period of time, before it is retracted and the catheter withdrawn. The radiation dose diminishes as a function of distance from the source train [10],[11]. Towards both ends of the source train, *fall-off zones* are present where subtherapeutic doses may be delivered. Given the differing penetration properties of β- and γ-energy, the radiation types vary in the degree of dose fall off, as well as their ability to effectively dose calcific and stented regions of the vessel [12]. Whenever the treated vessel segment exceeds the length covered by the train, the irradiation may be performed in subsegments (Fig. 2), which requires care when positioning the catheter to avoid over- or underdosing at the overlapping ends of the source trains. A detailed description of the different zones defined in intravascular brachytherapy can be found in [13].

This manuscript focuses on beta (β) radiation, where the application time is usually determined from source activity and the angiographically estimated vessel diameter. Conventionally, a simplified model is used, assuming a straight vessel with the catheter centered and a constant-diameter circular cross section. However, the irradiation pattern of the sources is complex [11]. Furthermore, vessel shape, curvature, and catheter location have a substantial impact on the actual dose delivered [10], [14], but are not considered in the current models of dose delivery. There is currently no universally accepted gold standard available for validating dose estimates since experimental methods frequently include distortions as well [11], [15]. The primary aim of this study was therefore to compare intravascular-brachytherapy dosing models using three-

This work has been supported in part by grant R01 HL63373 of the National Heart Lung and Blood Institute at NIH, Bethesda, MD 20892, USA. — *Asterisk indicates corresponding author.*

*A. Wahle is with the University of Iowa, Department of Electrical and Computer Engineering, Iowa City, IA 52242, USA (e-mail: a.wahle@ieee.org).

J. J. Lopez was with the University of Iowa, Department of Internal Medicine, Iowa City, IA 52242, USA; he is now with the University of Chicago, Department of Medicine, Chicago, IL 60637, USA.

E. C. Pennington, S. L. Meeks, and J. M. Buatti are with the University of Iowa, Department of Radiation Oncology, Iowa City, IA 52242, USA.

K. C. Braddy, T. M. H. Brennan, and J. D. Rossen are with the University of Iowa, Department of Internal Medicine, Iowa City, IA 52242, USA.

J. M. Fox was with the University of Iowa, Department of Internal Medicine, Iowa City, IA 52242, USA; he is now with the Grand Traverse Heart Associates, Traverse City, MI 49684, USA.

M. Sonka is with the University of Iowa, Department of Electrical and Computer Engineering, Iowa City, IA 52242, USA.

dimensional (3-D) computer simulations in an effort to estimate the influence of vessel shape and catheter position on dose distribution. To assess errors in delivered doses following the conventionally used dosing schemes, the actual differences in predicted dose distribution between a simplified tubular model and a geometrically correct 3-D model were quantified.

The studies described in this manuscript are based on the Novoste Beta-Cath system utilizing the Strontium/Yttrium ($^{90}\mathrm{Sr}/\mathrm{Y}$) β-isotope. In a 30–40 mm train, 12–16 sealed radiation sources are provided. The total dose accumulating at any given point of the vessel was estimated by using a fixed distance function derived from experimental data and the actually applied radiation parameters. Computer simulations were performed on a model considering parameters of vessel size and curvature as well as catheter position and straightness. Generation of the geometrically correct in-vivo model is a challenging task. Previous analyses of dose distribution were limited to single or stacked IVUS frames and did not always cover the full vessel segment that was irradiated [4], [5], [10]. Identification of the location of the source train was restricted to two-dimensional (2-D) interactive registration from angiograms [13]. While IVUS is well-suited to obtain high-resolution information about the cross-sectional vessel geometry and plaque composition [16], [17], it does not provide sufficient spatial information for an actual 3-D reconstruction. This fact results in the commonly used stacking of the frames regardless of the real vessel course in 3-D [10], [16]. X-ray angiography allows extraction of the vessel geometry from projectional images, e.g., for quantitative coronary angiography (QCA) [1], [18], [19], and also to obtain 3-D lumen reconstructions from biplane angiography [20]–[23]. However, angiography does not provide any directly visible information for the vessel wall, and the viewing angle substantially impacts accuracy of both 2-D and 3-D measurements due to foreshortening and overlapping [21], [24]. By fusion of the data from both modalities, the maximum of information can be extracted [1], [25]–[28].

To reconstruct the actual 3-D vessel geometry for our in-vivo studies, we combined the IVUS data obtained after PTCA and brachytherapy with the corresponding images from biplane angiography (Fig. 3) utilizing a well-established fusion system [28]–[30]. Figure 4 shows the fusion result for the patient introduced in the previous figures. A finite-element mesh was generated from the reconstructed vessel and then used as input for the brachytherapy simulation system. The results were statistically evaluated for the impact of vessel geometry and catheter position. On the in-vivo data, a comprehensive comparison between geometrically correct and simplified dose models was performed.

II. Methods

A. Dose-Distribution Model

The characteristics of the Novoste Beta-Cath β-radiation catheter used for brachytherapy at the University of Iowa Hospitals and Clinics were modeled from previously reported experiments on dose distribution [11]. The catheter consists of a hydraulic setup with 12 or 16 sources connected in a train. With a delivery device, this train can be moved from the protective container to the tip of the delivery catheter and retracted after the specified irradiation time has passed.

A one-dimensional distance function has been employed to simulate the dose fall-off, based on data from Soares, Halpern, and Wang for $^{90}\mathrm{Sr}/\mathrm{Y}$ radionuclides [11]. Their comprehensive data have been condensed to obtain a sufficiently accurate dose estimate with reasonable computational effort. For each source i, the dose in Gray (Gy) for any point p in a distance of d_{pi} was determined as follows:

$$D_i(d_{pi}) = \frac{C \cdot A_i \cdot t \cdot g(d_{pi})}{{d_{pi}}^2} \quad (1)$$

$$\text{with } g(d) = a_0 + a_1 \cdot d + a_2 \cdot d^2 + a_3 \cdot d^3 + a_4 \cdot d^4 \quad (2)$$

$$D_p = \sum_i D_i(d_{pi}) \quad (3)$$

where C is a dose rate constant specific for the brachytherapy device; A_i is the activity of the source in giga-Becquerels (GBq), with usually the same A_i for all i within a train; t is the application time in seconds; and $g(d)$ is a radial dose function with polynomial coefficients a_0 to a_4 derived from experimental results. The polynome has been validated for a range $0.75\,\mathrm{mm} \le d_{pi} \le 9.0\,\mathrm{mm}$. The minimum results from the diameter of the delivery catheter (5F = 1.6 mm). For distances above 9.0 mm, the dose was assumed to be zero. The total dose D_p for point p was determined as the sum of the individual doses delivered from all sources i.

As shown in Fig. 5, the shape of the simulated train source substantially affects the dose distribution. The above model assumes a *point* source, i.e., all radiation is emitted from the same point for each source. However, a source element is not accurately represented by just a single point. Expanding the source homogeneously over the length of a train element would not reflect the actual shape of the source either. Such a *linear* arrangement suggests a constant level of radiation at each distance. As a compromise of computational cost and model accuracy, the activity of a single source is distributed over the *active length* of the element. For the Novoste Beta-Cath system, this is 2.3 mm for each straight element of 2.5 mm total length. To simulate the active length while keeping the point-source model, the total activity A_i of a source is distributed over n_i equidistant subsources j with $A_{ij} = A_i/n_i$.

B. Computer Models

The basic shape of the computer phantom used for testing was a 50 mm tube with nine coaxial layers between 1.0 and 5.0 mm radius in 0.5 mm intervals, and was represented as a structured finite-element mesh. With respect to the world coordinate system defined in [22], [31], the tube was aligned along the y-axis. The longitudinal resolution of this shape was 10 μm, and the width of the radial segments 1°. The β-radiation catheter was simulated by a centered source train of 12 elements with 2.5 mm length each. The irradiation parameters

were taken from an actual patient with a prescribed dose (PD) of 18.4 Gy at 2 mm depth (C = 0.0164 Gy/GBqs, A_i = 0.136 GBq, and t = 180 sec). Note that the assumption of a single set of irradiation parameters is sufficient, since different values would only scale the dose distribution linearly.

To allow for a comprehensive set of scenarios, the catheter could be moved to an out-of-center or oblique position, or superimposed with a cosine-wave to provide varying out-of-center locations between the ends and the center portion. The resulting tubular coordinates $[x_s, y_s, z_s]$ were then mapped onto a torus segment with an enclosed angle of up to 180°. Importantly, the radius r of the torus depends on the angle $\kappa \in [0, \pi]$ of the enclosed segment. In the following, a vessel curvature of κ implies that r is chosen to yield the length l of the straight vessel over a torus segment with an enclosed angle of κ [Fig. 6(a)]. We simulated curvatures for κ of 0°, 60°, 120°, and 180° for a vessel length l of 50 mm. This model sufficiently represents curvatures commonly found in coronary arteries. To obtain a segment of a torus with radius r that corresponds to the desired curvature κ with the total length l preserved, the final vertex and β-source coordinates $[x_t, y_t, z_t]$ were determined by:

$$\begin{bmatrix} x_t \\ y_t \\ z_t \end{bmatrix} = \begin{bmatrix} (x_s + r) \cdot \cos(\varphi) - r \\ (x_s + r) \cdot \sin(\varphi) \\ z_s \end{bmatrix} \tag{4}$$

for $0 < \kappa \leq \pi$ with $r = l/\kappa$ and $\varphi = y_s/r$ [Fig. 6(a)]. For $\kappa = 0$, vector $[x_t, y_t, z_t]$ equals directly $[x_s, y_s, z_s]$. Since r was calculated relative to the centerline length l of the simulated vessel, the locations of the sources had to be recalculated when additional shifts or a cosine waveform were superimposed on the catheter path [Figs. 6(b), (c)]. This adjustment ensured their 2.5 mm spacing. The elements retained their shape in accordance with the physical properties of the real source elements, i.e., they were not bent with the curvature but rather aligned with the local centerline tangents.

C. 3-D Reconstruction of In-Vivo Data

The geometrically correct model of the irradiated vessel segment was generated using biplane angiography to extract the vessel geometry and IVUS to obtain cross-sectional information [29], [30]. IVUS imaging was performed using a 40 MHz CVIS ClearView system, and a biplane Philips Integris BH-5000 device was used for X-ray angiography. IVUS data were recorded on S-VHS tape and afterwards digitized, whereas the angiographic data were directly available in digital DICOM format. Physiological data (electrocardiography, ECG) for gating were recorded on the audio track of the tape as well as in the DICOM dataset. For imaging, the IVUS transducer was placed well distally of the treated area and its location imaged with biplane angiography (Fig. 3). The IVUS transducer was then pulled back at 0.5 mm/s using an automated pullback device. Filled with diluted contrast dye, the vessel lumen outline was also depicted in the angiograms and served as a reference for the 3-D matching of the orientation of the IVUS frames. The resulting data were sorted by heart phase according to the ECG signal, segmented for lumen/plaque and media/adventitia borders, and then mapped into 3-D space based upon the angiographically determined pullback trajectory (Fig. 4). In contrast to other systems [10], [16], the pullback was continuous and ECG-gating was performed as a post-processing step [32]. This keeps the imaging time in a clinically acceptable range while still delivering accurate data.

The location of a given IVUS frame results directly from its time-stamp along with the pullback speed, thus allowing one to calculate the pullback length completed when this specific frame was imaged. However, determination of the frame orientation is more complex and may be ambiguous [25]. We have employed a two-step solution to this problem. In the first step, changes in orientation from frame to frame were established analytically based on differential geometry, followed by a 3-D matching of the overall frame set against the angiographic outline of the vessel lumen [29], [30]. After the 3-D model of the vessel was available, the tissue enclosed by the segmented lumen/plaque and media/adventitia borders was represented using a structured finite-element mesh with 4 layers and 72 radial 5° segments per IVUS frame. Train length and radiation parameters were obtained from the patient file. The location of the brachytherapy catheter was estimated relative to the stented segment from the corresponding angiographic images (Fig. 2). Whenever biplane angiography with diluted contrast dye was also used for imaging the source train, its location was accurately established by 3-D measurement.

D. Simplified Tubular Model

To determine the impact of simplifications in widely used dosing models that assume a centric catheter and neglect the cross-sectional shape of the vessel, a simplified tubular model was created for each vessel. This model was directly derived from the 3-D geometrically correct model by straightening, centering of the catheter, and reshaping each contour to co-axial circles with the same per-frame mean diameters as determined from the original data. The computer-simulation tool presented in Section II-B was therefore modified to accept the 3-D geometry reconstructed with the fusion approach and to manipulate the tubular structure to match the longitudinal radius profile of the in-vivo data. To allow for an accurate comparison, the length and mesh resolution of the simplified tubular model was the same as for the corresponding geometrically correct model.

III. Results

A. Computer Models

Figure 5 shows the different source shapes that were tested. The irradiation parameters were chosen to obtain an 18.4 Gy dose at 2 mm. While the linear source produces an artificial homogeneity of 18.3887 ± 0.0001 Gy (mean ± standard deviation SD) in this depth, the point source overestimates the variability in dose as 18.3896 ± 0.1911 Gy. The approach to model the active length only (thus, 2.3 of 2.5 mm or 92%) yielded a dose estimate of 18.3889 ± 0.0166 Gy and was used in the following studies. Table I demonstrates the fall-off with increasing depth for the two center elements and the two border elements. Note that the standard deviation in the center decreases for depths

below approximately 4 mm and then increases again in more distant layers. This is due to the varying overlap between the different sources contributing to the total dose for each single point. For the same reason, the dose decreases more quickly in distant layers at the train borders than in the center region.

In the curved simulation with centered catheter [Figs. 6(a) and 7], the average dose at the outer curvature decreased by 7.48% to 17.014 Gy, while it was increased by 9.70% to 20.172 Gy at the innermost curvature for $\kappa = 180^\circ$ at 2 mm depth. A moderate curvature of 60° over the 50 mm vessel length resulted in a decrease of 2.70% at the outer and an increase of 2.95% at the inner curvature. The standard deviation on each side was contrary to the averages. For the 180° case, it was increased at the outer curvature to 0.0254 Gy and decreased to 0.0092 Gy at the inner curvature as compared to 0.0166 Gy in the straight vessel. This corresponds with the fact that the overlapping of the sources is stronger in the inner curvature as compared to the outer curvature.

Figures 8 and 9 demonstrate the dose changes when the catheter is not in the center of the vessel. As Table I shows, a difference of just 1 mm in location can roughly double or halve the dose delivered. Consequently, the doses can reach either 10 Gy or 40 Gy instead of the 18.4 Gy intended in these cases. To answer the question how out-of-center position of the catheter and the curvature work in combination, two scenarios were tested in the 120° torus (Fig. 9, lower panel): (1) at the center of the vessel, the catheter is eccentric towards the *inner* curvature of the vessel, and (2) the catheter is eccentric towards the *outer* curvature. To compensate for the fall-off zones and to have a longer segment covered, a 40 mm catheter was used in a 60 mm simulated vessel with a curvature of $\kappa = 120^\circ$. The inner-curvature scenario resulted in a peak dose at the 2 mm level of 40.956 Gy, whereas the outer-curvature resulted in a lower peak of 38.617 Gy. The inner/outer-curvature ratio was even stronger in 5 mm depth with 5.010 Gy vs. 4.289 Gy.

B. In-Vivo Patient Data

The current set of individuals in this ongoing study includes 8 patients treated with intravascular brachytherapy. The prescribed doses (PD) were determined from the visual estimate of the angiographic lumen size. The PD is still not well defined for coronary angioplasty [6] and is usually specified as a desired radiation level at a given distance from the source train. However, the vessel wall is considered as a volume rather than a single level, thus the PD definition is inherently insufficient. An individual target range is derived as a window around the PD that covers the expected range of doses between lumen/plaque and media/adventitia borders. In our set of patients, the individual PD values ranged from 18.4 to 25.3 Gy in a 2 mm distance from the radiation catheter. Considering that the therapeutic range of doses is between 12 and 30 Gy, the individual target range for each irradiation was defined as PD $\pm$ 5 Gy (i.e., from a minimum of $18-5 \geq 12$ Gy to a maximum of $25+5 \leq 30$ Gy). In two patients, two subsequent irradiations were performed at abutting locations to cover a longer segment of the restenotic vessel. Since the PD was different between the proximal and the distal segments in one of these patients, the irradiations were considered individually. Grids with 41,868 $\pm$ 14,942 points per vessel were generated. On average, 66% of grid points were located within the boundaries of the radiation source trains. The dose distribution for the patient presented in Figs. 1–4 is shown in Fig. 10 for the lumen/plaque and media/adventitia interfaces. There is obviously a high variation of doses delivered to each point of a contour, e.g., 4.73–38.7 Gy in frame #164 of the media/adventitia border.

In absolute values, 46.1% of the media/adventitia elements within the train boundaries received their dose target range. Underdosing (<10 Gy) occurred in 0.8% at the lumen/plaque and in 14.0% of elements at the media/adventitia borders. Overdosing (>30 Gy) was found in 6.3% of the media/adventitia elements. The variability across patients was also considerable; 16.9 to 68.7% of media/adventitia elements satisfied their individual target range for the specific patient.

C. Geometrically Correct vs. Simplified Model

All geometrically correct models were subsequently straightened as described in Section II-D. This process is illustrated in Fig. 11. The resulting dose chart has a visually-apparent smoother distribution. The dose histograms in Fig. 12 show that the doses are more concentrated to specific ranges in the simplified model than they are in the geometrically correct model. However, this result is typically seen only in vessels which maintain a relatively constant diameter over their entire length. Table II summarizes the comparison results between simplified tubular vs. the geometrically correct model. The tubular model resulted in significantly and systematically lower estimates of dose within the train boundaries ($p < 0.001$). The average dose estimate within the four layers was 3.04 Gy (lumen/plaque) to 1.13 Gy (media/adventitia), or 8.76 to 6.52%, respectively, lower as compared to the geometrically correct model. Note that the difference between the two models is larger in vessels with high overall curvature. The estimated doses differed significantly more in the right coronary artery segments than in the segments of the left coronary artery ($p < 0.001$; Table II, right panel). Even in the least curved vessel, the dose difference between geometrically correct and simplified tubular models was still statistically significant. In addition to the lower estimates of the mean dose for the tubular model, it also suggests a significantly lower level of dose variability than obtained from the geometrically correct model by ignoring vessel contour and catheter location ($p < 0.001$). The tubular model predicted standard deviations of dose from 5.11 Gy at the lumen/plaque interface to 3.71 Gy at the media/adventitia interface, thus substantially lower than the dose variations of 11.93 Gy and 6.72 Gy, respectively, as assessed by the geometrically correct model.

IV. Discussion

Our comprehensive analysis performed in computer simulations on phantoms and on a set of patients demonstrated that vessel curvature and out-of-center position of the delivery catheter have a substantial impact on the dose distribution. While previous reports have shown the influence of an eccentric catheter on circumferential dose variability in straightened vessel segments [4],[10], we performed a quantification of the dose

distribution in curved phantoms and in geometrically correct 3-D models derived from in-vivo patient data. Our results suggest that common assumptions made in conventional dose-delivery models introduce systematic and significant errors. However, it has to be kept in mind that a thorough validation in-vivo or ex-vivo that would include direct measurements of the actual doses delivered has not been performed thus far but will certainly be a focus in future research. Even though *absolute* dose values yet remain unvalidated, the *tendencies* derived from this study are obvious. Especially, the lower dose variability suggested by a simplified model as compared to a geometrically correct model is expected to remain valid regardless of absolute values.

The fusion-reconstruction model assumes that the delivery catheter follows the path of the IVUS catheter used for vessel imaging. This assumption is sufficiently accurate considering visual estimates of the brachytherapy catheter location in the angiographic images. Additionally, limitations and ambiguities of the IVUS data occasionally interfere with the accuracy of wall layer segmentation (lumen/plaque and especially the media/adventitia interfaces). While the first limitation can be overcome by using biplane angiography and diluted contrast dye imaging of the advanced brachytherapy catheter, the second problem is inherent to IVUS. For example, shadowing from calcified plaque obstructs recognition of the media on IVUS images, thus requiring interpolation of non-visualized segment locations. Similarly, this interface may be difficult to identify in stented areas due to compressed plaque and reverberations from the stent structures (Fig. 1). One focus of our ongoing research is the improvement of the IVUS segmentation methods to reduce the amount of manual corrections required [33].

Another desirable extension of our approach is to incorporate a more sophisticated dose model with the imaging parameters. The current dosimetry model assumes that all tissues have unit density. IVUS allows for detection of basic plaque tissue properties directly from the image data (soft and calcific plaque [17]). A recent study using radio-frequency IVUS reported improved sensitivity and specificity for plaque classification as compared to conventional IVUS imaging and also discrimination between early and advanced stages of plaque [34]. Therefore, the finite-element mesh representing the vessel wall could be extended to contain qualifiers for different tissue and plaque types. The dosimetric perturbations caused by calcified plaques and other tissue heterogeneities have been well documented [12], [14], [35]. Coupling tissue-characterization data from our geometrically correct 3-D reconstructions with a more sophisticated dose model, such as the EGSnrc Monte Carlo code [36], would provide a much more accurate representation of the actual doses delivered to patient-specific geometries. Dose-volume histograms as proposed in [10] can be calculated for each volume between two layers over an entire vessel segment or locally with one of the volumetric measurement methods described in [37].

The representation of the vessel as a finite-element structure could also be extended towards a 4-D modeling, i.e., 3-D plus time. We have already employed 4-D modeling in the quantification of local wall shear stress [32]. The influence of vessel motion on dose distribution was already addressed in [14], however not in 3-D space. In accordance with IVUS data, angiographic images, and a given tissue model, the movement of the vessel could be accurately reproduced. Furthermore, the 4-D model would consider any movement of the delivery catheter within the vessel over the heart cycle. This should be of special value in vessel segments with relatively low curvature, where the delivery catheter is not forced to rest against the vessel wall.

V. Conclusions

In intravascular brachytherapy, dose delivery depends on the shape and curvature of the vessel as well as on the position of the radiation catheter train within the vessel. Our simulation results obtained in this study imply that intravascular brachytherapy dose-assessment models that do not consider these factors suggest a significantly reduced dose variability. Compared to a geometrically correct model, the conventional models also provide on average lower values of radiation doses. Consequently, a significant percentage of tissue within the target zone at the media-adventitial area may not reach its prescribed dosing parameters. The existence of this dosing variability may result in less effective treatment, paradoxical stimulatory effects on the neointima, or overdosing resulting in tissue necrosis. Despite the current limitations in determination of the absolute dose delivered, the presented study improves the evaluation of potential shortcomings in clinical procedures. Our method to determine the dose at each point of the treated vessel segment in real 3-D from data fusion allows us to identify potential locations of over- or underdosing in the actual geometry of the patient's vessel. This will likely provide valuable input into changes of radiation protocols and possibly the design of future brachytherapy catheters.

Acknowledgments

The authors would like to thank Steven C. Mitchell and Mark E. Olszewski, graduate students in Electrical and Computer Engineering at the University of Iowa, for their contributions to the development of the image data fusion system for geometrically correct reconstruction of coronary arteries in vivo.

References

[1] J. H. C. Reiber, G. Koning, J. Dijkstra, A. Wahle, B. Goedhart, F. H. Sheehan, and M. Sonka, "Angiography and intravascular ultrasound," in *Handbook of Medical Imaging — Volume 2: Medical Image Processing and Analysis*, M. Sonka and J. M. Fitzpatrick, eds., Bellingham WA, pp. 711–808, SPIE Press, 2000.

[2] G. S. Mintz, J. J. Popma, A. D. Pichard, K. M. Kent, L. F. Satler, S. C. Wong, M. K. Hong, J. A. Kovach, and M. B. Leon, "Arterial remodeling after coronary angioplasty: A serial intravascular ultrasound study," *Circulation*, vol. 94, no. 1, pp. 35–43, July 1996.

[3] R. E. Kuntz and D. S. Baim, "Prevention of coronary restenosis: The evolving evidence base for radiation therapy," *Circulation*, vol. 101, no. 18, pp. 2130–2133, May 2000.

[4] M. Sabaté, J. P. A. Marijnissen, S. G. Carlier, I. P. Kay, W. J. van der Giessen, V. L. M. A. Coen, J. M. R. Ligthart, E. Boersma, M. A. Costa, P. C. Levendag, and P. W. Serruys, "Residual plaque burden, delivered dose, and tissue composition predict 6-month outcome after balloon angioplasty and β-radiation therapy," *Circulation*, vol. 101, no. 21, pp. 2472–2477, May 2000.

[5] G. S. Mintz, N. J. Weissman, and P. J. Fitzgerald, "Intravascular ultrasound assessment of the mechanisms and results of brachytherapy," *Circulation*, vol. 104, no. 11, pp. 1320–1325, Sept. 2001.

[6] R. A. Fox, "Intravascular brachytherapy of the coronary arteries," *Physics in Medicine and Biology*, vol. 47, no. 4, pp. R1–R30, Feb. 2002.

[7] R. Waksman, B. Bhargava, J. F. Saucedo, R. C. Chan, F. O. Tio, Y. Vodovotz, and V. Verin, "Yttrium-90 delivered via a centering catheter and afterloader, given both before and after stent implantation, inhibits neointima formation in porcine coronary arteries," *Cardiovascular Radiation Medicine*, vol. 2, no. 1, pp. 11–17, Jan.-Mar. 2000.

[8] H. C. Lowe, C. N. Chestman, and L. M. Khachigian, "Rat aortic stenting: Toward a simple model of in-stent restenosis," *American Journal of Cardiology*, vol. 88, no. 6, pp. 720–721, Sept. 2001.

[9] A. J. M. Roks, R. H. Henning, A. J. van Boven, R. A. Tio, and W. H. van Gilst, "Rat abdominal aortic stenting: A simple model displaying in-stent restenosis," *American Journal of Cardiology*, vol. 89, no. 9, pp. 1149–1150, May 2002.

[10] S. G. Carlier, J. P. A. Marijnissen, V. L. M. A. Coen, W. J. van der Giessen, M. Sabaté, J. M. R. Ligthart, A. den Boer, I. E. Céspedes, W. Li, A. F. W. van der Steen, P. C. Levendag, and P. W. Serruys, "Guidance of intracoronary radiation therapy based on dose-volume histograms derived from quantitative intravascular ultrasound," *IEEE Transactions on Medical Imaging*, vol. 17, no. 5, pp. 772–778, Oct. 1998.

[11] C. G. Soares, D. G. Halpern, and C. K. Wang, "Calibration and characterization of β-particle sources for intravascular brachytherapy," *Medical Physics*, vol. 25, no. 3, pp. 339–346, Mar. 1998.

[12] X. A. Li, R. Wang, C. Yu, and M. Suntharalingam, "Beta versus gamma for catheter-based intravascular brachytherapy: Dosimetric perspectives in the presence of metallic stents and calcified plaques," *International Journal of Radiation Oncology · Biology · Physics*, vol. 46, no. 4, pp. 1043–1049, Mar. 2000.

[13] G. Koning, J. C. Tuinenburg, E. Hekking, J. Peelen, A. van Weert, D. Bergkamp, B. Goedhart, and J. H. C. Reiber, "A novel measurement technique to assess the effects of coronary brachytherapy in clinical trials," *IEEE Transactions on Medical Imaging*, vol. 21, no. 10, pp. 1254–1263, Oct. 2002.

[14] V. Sehgal, Z. Li, J. R. Palta, and W. E. Bolch, "Dosimetric effect of source centering and residual plaque for β-emitting catheter-based intravascular brachytherapy sources," *Medical Physics*, vol. 28, no. 10, pp. 2162–2171, Oct. 2001.

[15] R. Nath, H. I. Amols, C. W. Coffey, D. M. Duggan, S. K. Jani, Z. Li, M. C. Schell, C. G. Soares, J. S. Whiting, P. E. Cole, I. R. Crocker, and R. S. Schwartz, "Intravascular brachytherapy physics: Report of the AAPM radiation therapy committee task group #60," *Medical Physics*, vol. 26, no. 2, pp. 119–152, Feb. 1999.

[16] C. von Birgelen, E. A. de Vrey, G. S. Mintz, A. Nicosia, N. Bruining, W. Li, C. J. Slager, J. R. T. C. Roelandt, P. W. Serruys, and P. J. de Feyter, "ECG-gated three-dimensional intravascular ultrasound: Feasibility and reproducibility of the automated analysis of coronary lumen and atherosclerotic plaque dimensions in humans," *Circulation*, vol. 96, no. 9, pp. 2944–2952, Nov. 1997.

[17] X. Zhang, C. R. McKay, and M. Sonka, "Tissue characterization in intravascular ultrasound images," *IEEE Transactions on Medical Imaging*, vol. 17, no. 6, pp. 889–899, Dec. 1998.

[18] R. L. Kirkeeide, P. Fung, R. W. Smalling, and K. L. Gould, "Automated evaluation of vessel diameter from arteriograms," in *Proc. Computers in Cardiology 1982*, Los Alamitos CA, pp. 215–218, IEEE-CS Press, 1982.

[19] P. J. de Feyter, P. W. Serruys, M. J. Davies, P. Richardson, J. Lubsen, and M. F. Oliver, "Quantitative coronary angiography to measure progression and regression of coronary atherosclerosis; value, limitations, and implications for clinical trials," *Circulation*, vol. 84, no. 1, pp. 412–423, July 1991.

[20] C. Seiler, R. L. Kirkeeide, and K. L. Gould, "Basic structure-function relations of the epicardial coronary vascular tree; basis of quantitative coronary arteriography for diffuse coronary artery disease," *Circulation*, vol. 85, no. 6, pp. 1987–2003, June 1992.

[21] A. Wahle, E. Wellnhofer, I. Mugaragu, H. U. Sauer, H. Oswald, and E. Fleck, "Assessment of diffuse coronary artery disease by quantitative analysis of coronary morphology based upon 3-D reconstruction from biplane angiograms," *IEEE Transactions on Medical Imaging*, vol. 14, no. 2, pp. 230–241, June 1995.

[22] A. Wahle, H. Oswald, and E. Fleck, "3-D heart-vessel reconstruction from biplane angiograms," *IEEE Computer Graphics and Applications*, vol. 16, no. 1, pp. 65–73, Jan. 1996.

[23] E. Wellnhofer, A. Wahle, and E. Fleck, "Progression of coronary atherosclerosis quantified by analysis of 3-D reconstruction of left coronary arteries," *Atherosclerosis*, vol. 160, no. 2, pp. 483–493, Feb. 2002.

[24] S. Y. J. Chen and J. D. Carroll, "3-D reconstruction of coronary arterial tree to optimize angiographic visualization," *IEEE Transactions on Medical Imaging*, vol. 19, no. 4, pp. 318–336, Apr. 2000.

[25] M. Laban, J. A. Oomen, C. J. Slager, J. J. Wentzel, R. Krams, J. C. H. Schuurbiers, A. den Boer, C. von Birgelen, P. W. Serruys, and P. J. de Feyter, "ANGUS: A new approach to three-dimensional reconstruction of coronary vessels by combined use of angiography and intravascular ultrasound," in *Proc. Computers in Cardiology 1995*, Piscataway NJ, pp. 325–328, IEEE Press, 1995.

[26] J. L. Evans, K. H. Ng, S. G. Wiet, M. J. Vonesh, W. B. Burns, M. G. Radvany, B. J. Kane, C. J. Davidson, S. I. Roth, B. L. Kramer, S. N. Meyers, and D. D. McPherson, "Accurate three-dimensional reconstruction of intravascular ultrasound data; spatially correct three-dimensional reconstructions," *Circulation*, vol. 93, no. 3, pp. 567–576, Feb. 1996.

[27] C. Pellot, I. Bloch, A. Herment, and F. Sureda, "An attempt to 3-D reconstruct vessel morphology from X-ray projections and intravascular ultrasounds modeling and fusion," *Computerized Medical Imaging and Graphics*, vol. 20, no. 3, pp. 141–151, May/June 1996.

[28] G. P. M. Prause, S. C. DeJong, C. R. McKay, and M. Sonka, "Towards a geometrically correct 3-D reconstruction of tortuous coronary arteries based on biplane angiography and intravascular ultrasound," *International Journal of Cardiac Imaging*, vol. 13, no. 6, pp. 451–462, Dec. 1997.

[29] A. Wahle, G. P. M. Prause, S. C. DeJong, and M. Sonka, "Geometrically correct 3-D reconstruction of intravascular ultrasound images by fusion with biplane angiography — methods and validation," *IEEE Transactions on Medical Imaging*, vol. 18, no. 8, pp. 686–699, Aug. 1999.

[30] A. Wahle, G. P. M. Prause, C. von Birgelen, R. Erbel, and M. Sonka, "Fusion of angiography and intravascular ultrasound in-vivo: Establishing the absolute 3-D frame orientation," *IEEE Transactions on Biomedical Engineering*, vol. 46, no. 10, pp. 1176–1180, Oct. 1999.

[31] H. Wollschläger, P. Lee, A. Zeiher, U. Solzbach, T. Bonzel, and H. Just, "Mathematical tools for spatial computations with biplane isocentric X-ray equipment," *Biomedizinische Technik*, vol. 31, no. 5, pp. 101–106, May 1986.

[32] A. Wahle, S. C. Mitchell, S. D. Ramaswamy, K. B. Chandran, and M. Sonka, "Four-dimensional coronary morphology and computational hemodynamics," in *Medical Imaging 2001: Image Processing*, M. Sonka and K. M. Hanson, eds., vol. 4322, Bellingham WA, pp. 743–754, SPIE Proceedings, 2001.

[33] S. C. Mitchell, J. G. Bosch, B. P. F. Lelieveldt, R. J. van der Geest, J. H. C. Reiber, and M. Sonka, "3-D active appearance models: Segmentation of cardiac MR and ultrasound images," *IEEE Transactions on Medical Imaging*, vol. 21, no. 9, pp. 1167–1178, Sept. 2002.

[34] P. M. Stähr, T. Höfflinghaus, T. Voigtländer, B. K. Courtney, A. Victor, M. Otto, P. G. Yock, R. Brennecke, and P. J. Fitzgerald, "Discrimination of early/intermediate and advanced/complicated coronary plaque types by radiofrequency intravascular ultrasound analysis," *American Journal of Cardiology*, vol. 90, no. 1, pp. 19–23, July 2002.

[35] V. Sehgal, Z. Li, J. R. Palta, K. M. Smith, and W. E. Bolch, "Application of imaging-derived parameters to dosimetry of intravascular brachytherapy sources: Perturbation effects of residual plaque burden," *Medical Physics*, vol. 29, no. 7, pp. 1580–1589, July 2002.

[36] R. Wang and X. A. Li, "Monte Carlo dose calculations of β-emitting sources for intravascular brachytherapy: A comparison between EGS4, EGSnrc, and MCNP," *Medical Physics*, vol. 28, no. 2, pp. 134–141, Feb. 2001.

[37] R. Medina, A. Wahle, M. E. Olszewski, and M. Sonka, "Volumetric quantification of coronary arteries reconstructed by fusion between intravascular ultrasound and biplane angiography," in *Proc. 2002 IEEE International Symposium on Biomedical Imaging*, Piscataway NJ, pp. 891–894, IEEE Press, 2002.

TABLE I

DOSE DISTRIBUTION FOR EACH LAYER OF A STRAIGHT VESSEL WITH A PRESCRIBED DOSE PD = 18.4 GY AT 2 MM FOR CENTER AND BORDER ELEMENTS; THE FALL-OFF ZONES OUTSIDE THE TRAIN BOUNDARIES HAVE BEEN DISCARDED.

Depth [mm]	Train Center (mean $\pm$ standard deviation) [Gy]	Train Border (mean $\pm$ standard deviation) [Gy]
1.0	39.898 ± 0.32342	31.270 ± 4.930
1.5	26.405 ± 0.06962	19.835 ± 3.153
2.0	18.389 ± 0.01656	13.411 ± 2.110
2.5	13.069 ± 0.00430	9.329 ± 1.443
3.0	9.345 ± 0.00126	6.567 ± 0.998
3.5	6.665 ± 0.00039	4.630 ± 0.692
4.0	4.713 ± 0.00009	3.247 ± 0.480
4.5	3.286 ± 0.00023	2.251 ± 0.330
5.0	2.247 ± 0.00032	1.534 ± 0.224

TABLE II

COMPARISON BETWEEN GEOMETRICALLY CORRECT MODEL GCM AND SIMPLIFIED TUBULAR MODEL STM OVER ALL 10 VESSEL SEGMENTS. NOTE THAT SD HERE IS THE MEAN INDIVIDUAL STANDARD DEVIATION OF ALL SEGMENTS AND THEREFORE NOT AFFECTED BY DIFFERENT PRESCRIBED DOSES PD. THE %-REDUCTION OF ESTIMATED DOSES STM VS. GCM IS LISTED SEPARATELY FOR THE THREE MAIN VESSELS.

Layer	GCM [Gy] (mean$\pm$SD)	STM [Gy] (mean$\pm$SD)	Difference means [%GCM]			
			All	LAD	LCX	RCA
	$n = 10$	$n = 10$	$n = 10$	$n = 3$	$n = 2$	$n = 5$
Lumen/Plaque	34.70 ± 11.93	31.66 ± 5.11	8.76	6.54	7.62	10.44
Intermediate 1	26.71 ± 8.76	24.85 ± 4.14	6.96	4.77	6.58	8.38
Intermediate 2	21.28 ± 7.41	19.92 ± 3.84	6.39	3.95	6.70	7.74
Media/Adven.	17.31 ± 6.72	16.18 ± 3.71	6.52	3.82	7.35	7.86

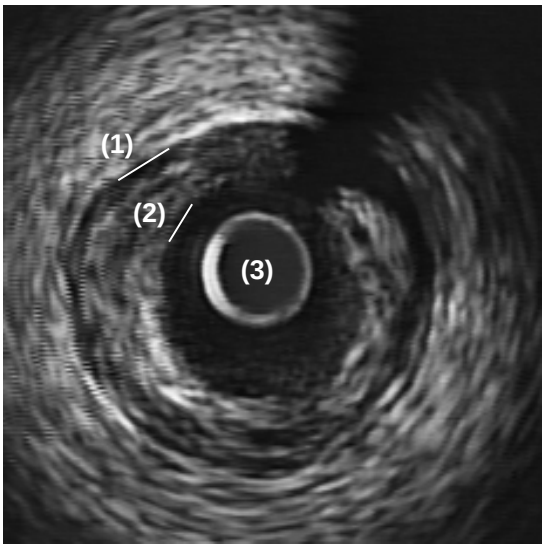

(a)

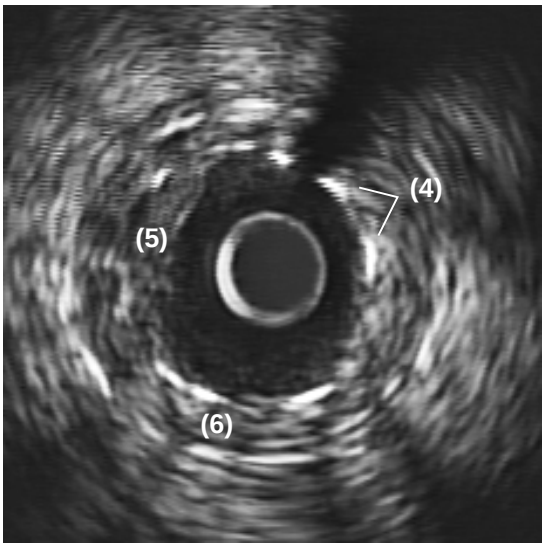

(b)

Fig. 1. Intravascular ultrasound images of a patient's right coronary artery with in-stent restenosis after PTCA and β-radiation treatment: (a) unstented vessel segment, (b) segment with stent; (1) media/adventitia interface, (2) lumen/plaque interface, (3) 2.9F imaging catheter, (4) stent struts, (5) plaque accumulation from in-stent restenosis, (6) plaque compressed during PTCA.

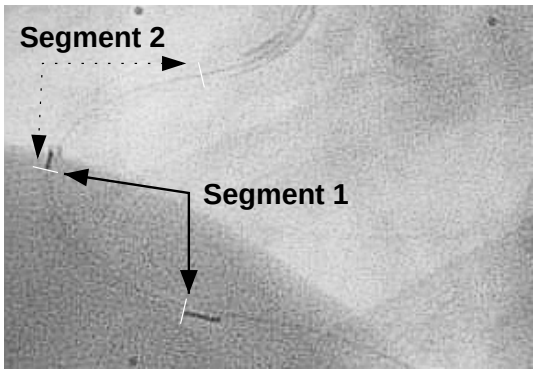

Fig. 2. In this case, brachytherapy was performed in two adjacent locations with a 12-source 30 mm β-catheter and identical irradiation parameters; note that only the markers are visible in the angiograms, which are not part of the active area.

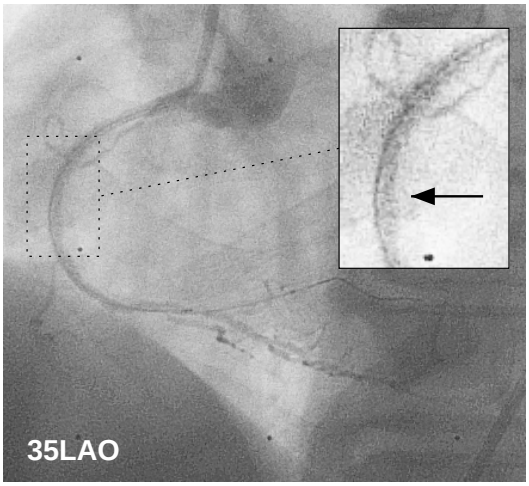

Fig. 3. Biplane angiographic images of the artery depicted in Fig. 1 showing the IVUS catheter before the pullback start; note the out-of-center position of the catheter.

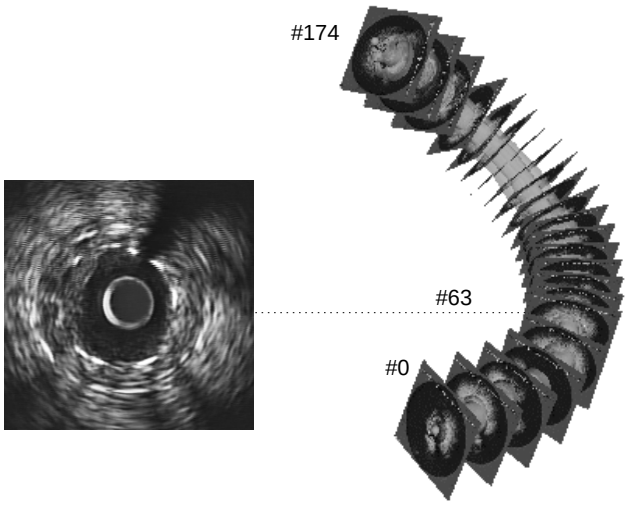

Fig. 4. Result of the fusion between the IVUS set from Fig. 1 and the angiograms in Fig. 3 from a posterior view; some IVUS frames have been inserted for illustration of the mapping process (frame numbering in direction of the IVUS pullback).

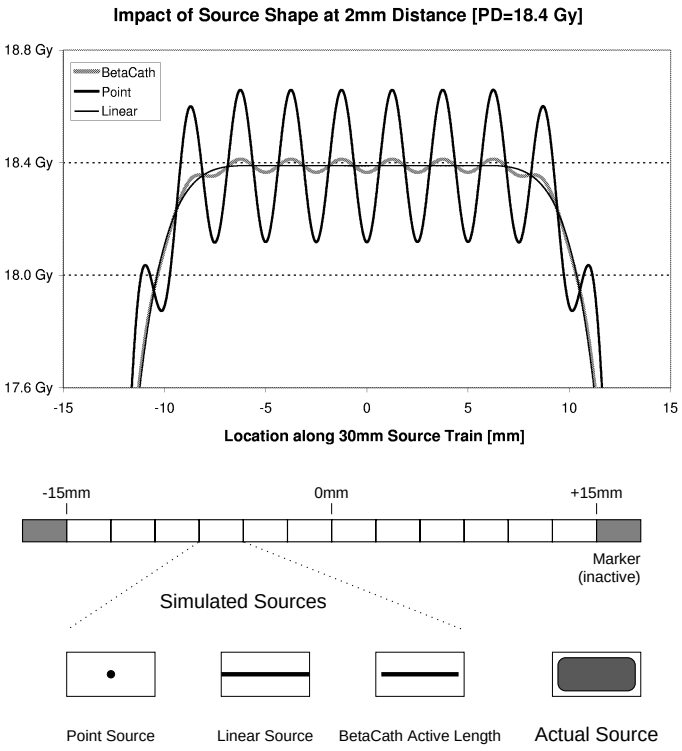

Fig. 5. Impact of the shape and active area of the simulated source on the heterogeneity of the dose distribution; the prescribed dose (PD) was derived from actual in-vivo calculations.

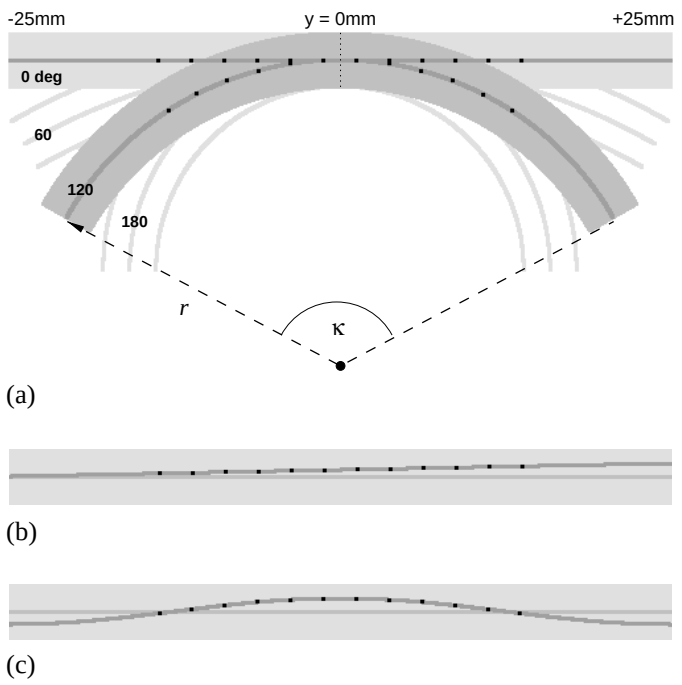

Fig. 6. Simulated vessel (a) for κ of 0°, 60°, 120°, and 180°, with sources shown for 0° and 120°, (b) displacement by 1 mm towards the positive y-axis, and (c) cosine wave with 1 mm amplitude; the shaded area indicates the 2 mm distance range in the x/y-plane.

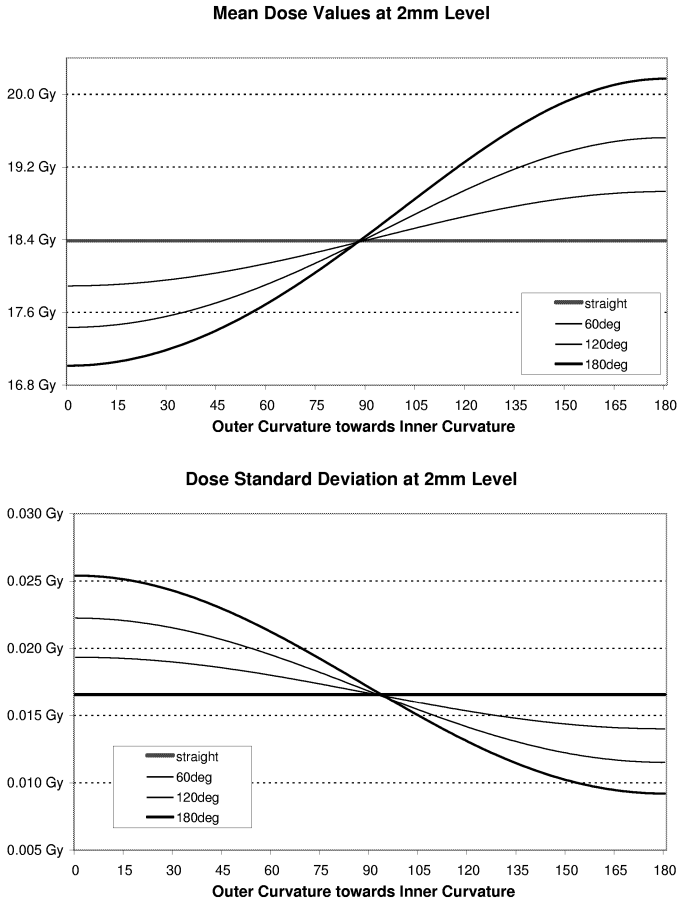

Fig. 7. Simulated vessels in Fig. 6(a) with a prescribed dose of PD = 18.4 Gy; the 0° angle corresponds to the outer side of the curvature, wheras the 180° angle corresponds to the inner side of the curvature.

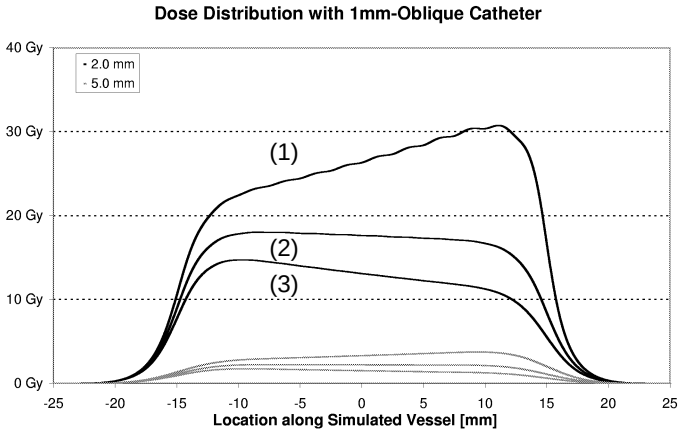

Fig. 8. Dose distribution of the oblique catheter as shown in Fig. 6(b), where the three lines represent top-down (1) the points on the vessel side the catheter is moving to, (2) the points on the vessel wall which are orthogonal to the catheter movement, and (3) the points on the vessel side the catheter is moving away from; note that the dose is reduced by the fall-off zones before reaching the actual 1 mm eccentric position.

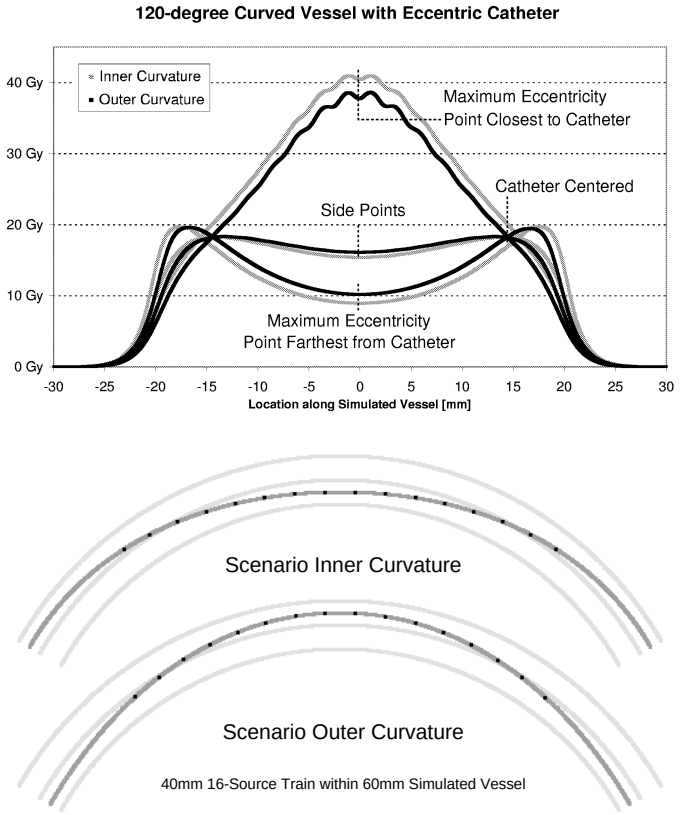

Fig. 9. Combination of the 120° torus segment shown in Fig. 6(a) with the cosine waveform from Fig. 6(c); if the eccentricity is directed towards the inner curvature, the effects of curvature and eccentricity are combined, whereas they are partially offsetting each other when the eccentricity tends towards the outer curvature.

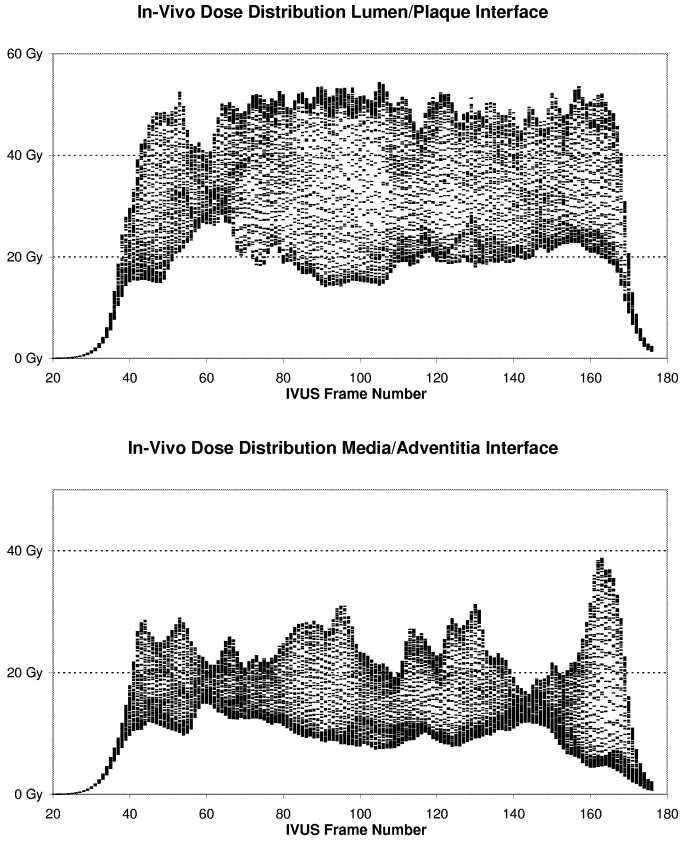

Fig. 10. Dose distribution in the in-vivo example for the innermost and outermost layer, with 72 circumferential grid points per contour and 134 contours over the 60 mm irradiated segment.

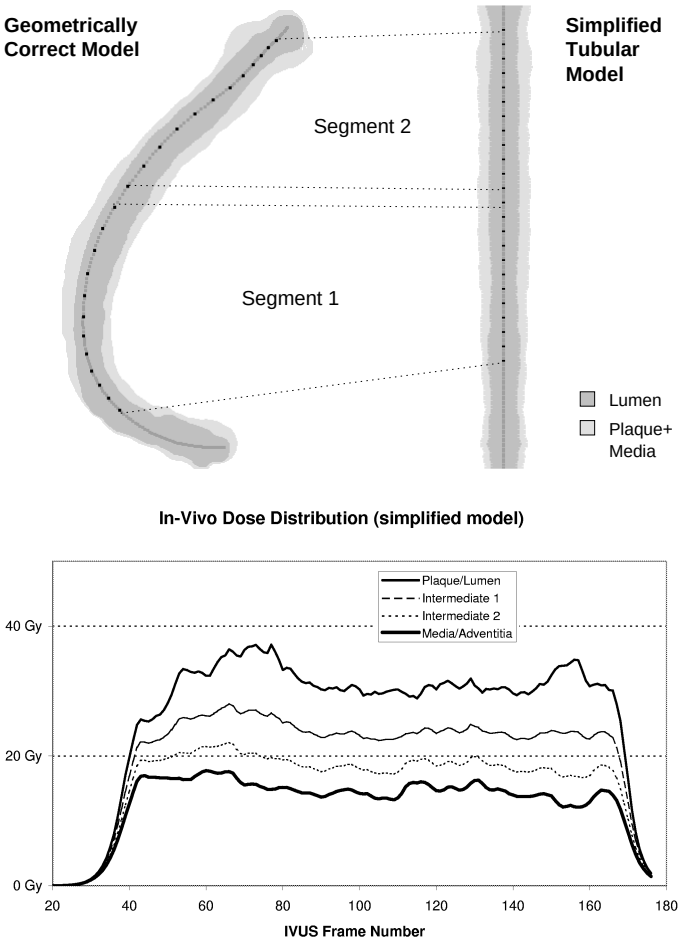

Fig. 11. Generation of the simplified tubular model from the 3-D fusion and corresponding dose distribution; due to the circular shape, all points within a contour receive the same dose.

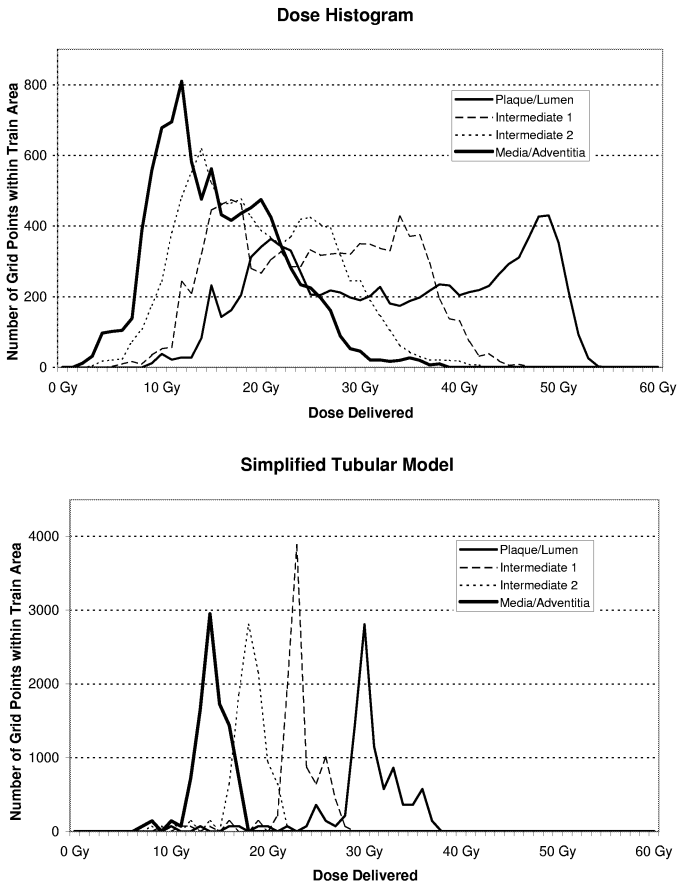

Fig. 12. Dose histograms summarizing the results shown in Figs. 10/11 for all four layers in both the geometrically correct and simplified tubular models.

Andreas Wahle (M'97–SM'03) received M.Sc. and Ph.D. degrees in Computer Science and Engineering from the Department of Computer Science at the Technical University of Berlin, Germany, in 1991 and 1997, respectively. He currently holds the rank of a Research Assistant Professor at the University of Iowa and is with the Department of Electrical and Computer Engineering since 1997. Main focus of his research are the spatio-temporal reconstruction of vascular structures by fusion between biplane angiography and intravascular ultrasound along with morphological and hemodynamical evaluations thereon. Further topics of interest include medical image processing, interactive visualization, image archiving and communication standards. Dr. Wahle is a member of the IEEE Engineering in Medicine and Biology Society, the IEEE Computer Society, and SPIE.

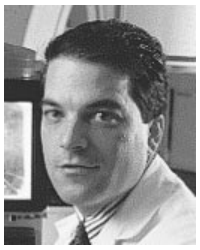

John J. Lopez received an M.D. degree from medical school at Columbia University College of Physicians and Surgeons in 1989 and afterwards performed his internal medicine and cardiology training at Beth Israel Hospital in Boston. At the University of Iowa, he was the Associate Director of Cardiac Catheterization and Interventional Cardiology, and the director of the interventional cardiology fellowship training program. He is now an Associate Professor of Medicine at the University of Chicago and the Director of Cardiac Catheterization and Interventional Cardiology. Dr. Lopez has been active in clinical and preclinical studies of therapeutic angiogenesis. His research interests also include IVUS, novel revascularization strategies for patients with advanced coronary artery disease, and new device studies for treatment of coronary artery disease.

Edward C. Pennington is a physicist and received his M.Sc. degree in Radiological Physics from the University of Texas Health Science Center in Dallas in 1980. Mr. Pennington has over 20 years experience in clinical radiotherapy. He has been with the University of Iowa's Radiation Therapy program since 1985 where he holds an associate position. He has co-authored numerous papers on various topics in Radiation Therapy Physics. His interests include radiation therapy treatment planning and verification, intensity-modulated radiation therapy, stereotactic radiation therapy and brachytherapy. He is a member of the American Association of Physicists in Medicine (AAPM).

Sanford L. Meeks received his M.Sc. degree in Physics from Florida State University in 1991 and his Ph.D. degree in Medical Physics from the University of Florida in 1994. He is Associate Professor of Radiation Oncology and holds a joint appointment in the Department of Biomedical Engineering at the University of Iowa. His primary research interests include stereotactic and image-guided radiation therapy. He is a member of the American Association of Physicists in Medicine, the American Society for Therapeutic Radiation Oncology, the American College of Radiology, and the International Stereotactic Radiosurgery Society.

Kathleen C. Braddy received an M.D. degree from the University of Colorado in 1997. She completed her internal medicine residency at the University of Iowa. Dr. Braddy is currently an interventional cardiology fellow at the University of Iowa. Her research interests include interventional device trials for treatment of coronary artery disease and studies investigating the effects of diabetes on coronary artery disease progression and treatment. She is a member of the American College of Cardiology and the American Heart Association.

James M. Fox received his M.D. in 1994 from the University of Pittsburgh. He completed his internship, residency, as well as fellowships in Cardiology and Interventional Cardiology at the University of Iowa Hospitals and Clinics. In addition, he is a Ph.D. candidate in Neurosciences from the California Institute of Technology. Dr. Fox's professional interests include all aspects of interventional cardiology, critical care cardiology and echocardiography. He is a member of the American College of Cardiology. He recently left the University of Iowa Hospitals and Clinics and joined the Grand Traverse Heart Associates in Michigan.

Theresa M. H. Brennan received an M.D. degree from Northwestern University Feinberg School of Medicine in 1992. She completed her Internal Medicine residency, cardiology fellowship, and interventional cardiology fellowship at the University of Iowa. Dr. Brennan is presently Assistant Professor of Internal Medicine and Director of Clinical Cardiovascular Services at the University of Iowa Healthcare. Her clinical interests include prevention of cardiovascular disease, treatment of peripheral arterial disease, and interventional cardiology. Her research interests include the study of the use of novel devices for catheter-based treatment of cardiovascular disease, treatment of patients with non-revascularizable cardiovascular disease including angiogenesis, and medical and interventional therapy for patients with peripheral arterial disease.

John M. Buatti earned his M.D. degree at Georgetown University in Washington, D.C., in 1986. He completed residency in Internal Medicine at Georgetown, followed by a residency in Radiation Oncology at the University of Arizona. Since 2001 he is the first Professor and Head of the newly created Department of Radiation Oncology at the University of Iowa. His active research and jointly held patents are related to the utilization of optic guidance for digital localization in radiotherapy. His main focus is creating the Center of Excellence for Image Guided Radiation Therapy, a new facility that will enable full utilization of technology potentials for the improvement of cancer therapy. Dr. Buatti is an internationally recognized expert in the management of brain tumors and radiosurgery. He received numerous awards and is affiliated with several major radiological societies.

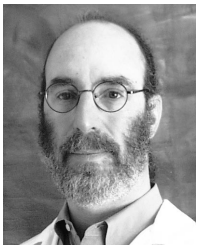

James D. Rossen received an M.D. degree from the Pritzker School of Medicine at the University of Chicago in 1980. He completed Internal Medicine residency and fellowships in Cardiology and Clinical Pharmacology at the University of Chicago. Dr. Rossen is Associate Professor and the Director of the Adult Cardiac Catheterization Laboratory and Interventional Cardiology at the University of Iowa Hospitals and Clinics. His research interests include regulation of the coronary circulation in pathophysiologic states, physiologic assessment of coronary artery lesions, and novel devices for catheter-based treatment of cardiac disease. He is a fellow of the American College of Cardiology and of the American Heart Association Council on Clinical Cardiology.

Milan Sonka (M'94–SM'00–F'02) received the Ph.D. degree from the Czech Technical University in Prague, Czechoslovakia, in 1983. He is Professor of Electrical and Computer Engineering at the University of Iowa. His research interests include knowledge-based medical image analysis. He is the first author of Image Processing, Analysis, and Machine Vision (London, U.K.: Chapman and Hall, 1993; 2nd ed. Pacific Grove, CA: PWS). He has co-authored Handbook of Medical Imaging, Volume II: Medical Image Processing and Analysis (Bellingham, WA: SPIE, 2000), several other books, and numerous journal and conference papers. Dr. Sonka is an Associate Editor of the IEEE TRANSACTIONS ON MEDICAL IMAGING and a Member of the Editorial Board of the International Journal of Cardiovascular Imaging.